



Distribution alignment for cross-device palmprint recognition

Lei Shen^{a,1}, Yingyi Zhang^{a,1}, Kai Zhao^{a,b,*}, Ruixin Zhang^a, Wei Shen^c

^a Tencent Youtu Lab, China

^b University of California, Los Angeles, USA

^c Shanghai Jiaotong University, China

ARTICLE INFO

Article history:

Received 17 October 2021

Revised 8 June 2022

Accepted 25 July 2022

Available online 30 July 2022

Keywords:

Palmprint recognition

Deep learning

Loss function

Biometric recognition

Person Reidentification

ABSTRACT

With the development of IoT and mobile devices, cross-device palmprint recognition is becoming an emerging research topic in multimedia for its great application potential. Due to the diverse characteristics of different devices, e.g. resolution or artifacts caused by post-processing, cross-device palmprint recognition remains a challenging problem. In this paper, we make efforts to improve cross-device palmprint recognition in two aspects: (1) we put forward a novel distribution-based loss to narrow the representation gap across devices, and (2) we establish a new cross-device benchmark based on existing palmprint recognition datasets. Different from many recent studies that only utilize instance-level or pairwise-level information between devices, the proposed progressive target distribution loss (PTD loss) uses the distributional information. Moreover, we establish a *progressive target* mechanism that will be dynamically updated during training, making the optimization easier and smoother. The newly established benchmark contains more samples and more types of IoT devices than previous benchmarks, which can facilitate cross-device palmprint research. Extensive comparisons on several benchmarks reveal that: (1) our method outperforms other cross-device biometric recognition approaches significantly; (2) our method presents superior performance compared to SOTA competitors on several general palmprint recognition benchmarks; Code and data are openly available at <https://kaizhao.net/palmprint>.

© 2022 Elsevier Ltd. All rights reserved.

1. Introduction

Recently, the palm payment device being developed by Amazon [1] has attracted people's attention. Compared with card payments, palm payments will significantly reduce the waiting time and bring great convenience to people. And the safety of the palmprint recognition system has been confirmed by numerous previous studies [2]. A successful palm payment system will revolutionize the way we do our shopping and significantly impact our daily life in the coming years.

During the last decade, palmprint recognition has switched from early contact and restricted images to unrestricted contactless images. And recently, some studies deal with images taken by mobile phones, such as MPD [3] and XJTU-UP [4]. However, besides smartphones, the devices used in payment application scenarios are diverse and include various IoT devices, such as the aforementioned AmazonOne [1]. Cross-device registration and identification improve payment convenience more effectively. For instance, customers can use their smartphones to register at home and use IoT

devices to complete identification and payment at stores. Yet, the heterogeneous visual characteristics between images across devices pose a huge challenge. Existing methods, such as ArcPalm [3], do not take into account the situation of domain shift, which leads to their poor performance in cross-device recognition scenarios.

As shown in Fig. 1 (a) and (b), pictures taken by different devices vary greatly in appearance. Consequently, as illustrated in Fig. 1 (c), though belonging to the same identity, images from different devices present large intra-class variance in the embedding space. This will largely affect the recognition performance on unseen data. To alleviate this problem, we propose a novel loss function, namely Progressive Target Distribution loss (PTD loss), that minimizes the distributional gap between cross-device and within-device similarities. Specifically, we estimate the histogram of similarity scores and minimize the distributional distance between the estimated histogram and target distribution. Our innovation is reflected in our proposed 'progress target'. Instead of setting up a fixed target, we propose the 'progressive target' that adjusts to each individual mini-batch.

Additionally, there are not sufficient datasets for cross-device RGB palmprint recognition. We collect a new cross-device palmprint recognition benchmark based on existing palmprint recognition datasets. The newly collected dataset consists of RGB images

* Corresponding author.

E-mail address: kz@kaizhao.net (K. Zhao).

¹ These contributed equally to this work.

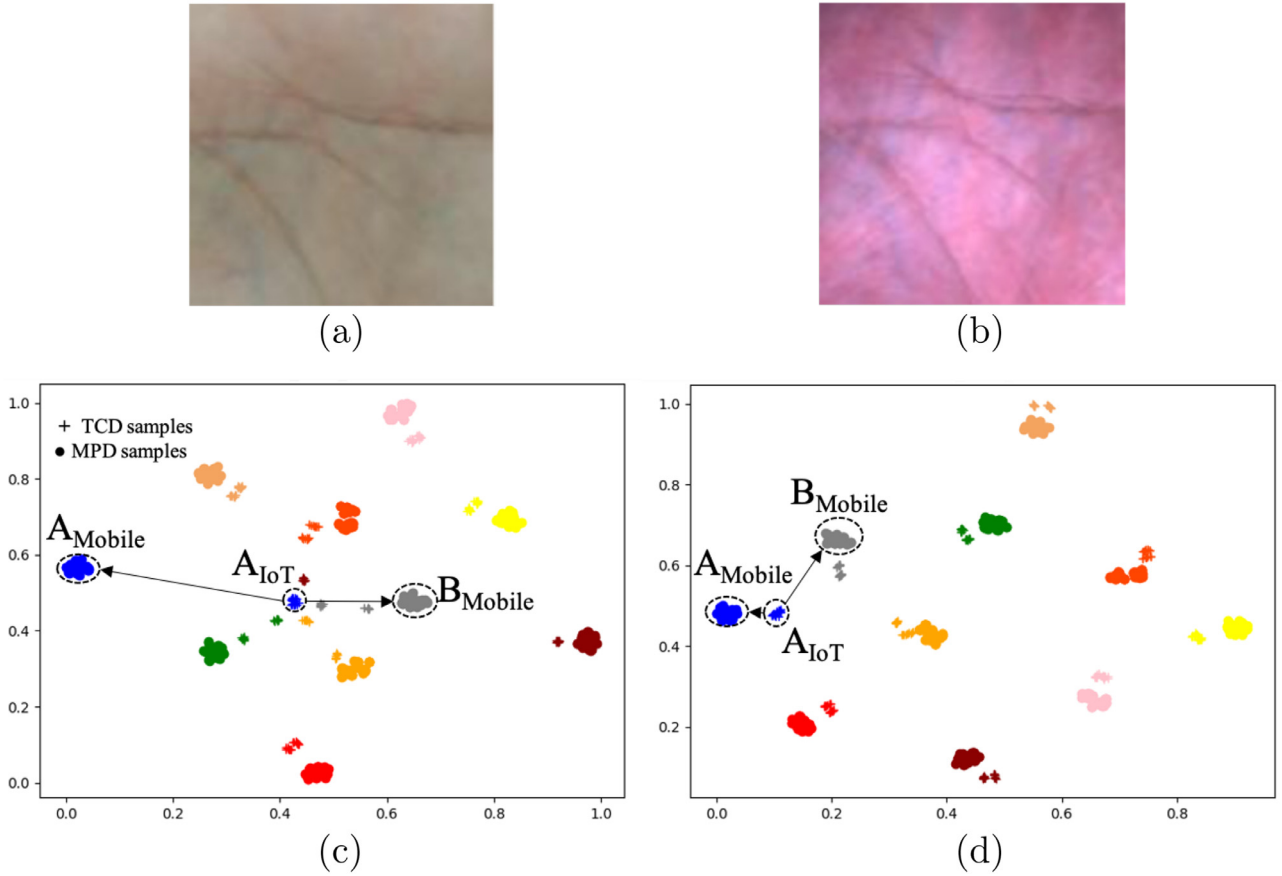


Fig. 1. Top: Images taken by mobile phones (a) and IoT devices (b) are diverse in appearance. Bottom: TSNE of palm features extracted by ArcPalm [3] (c) and our proposed method (d). Our method can shorten the distance between samples of the same identity but different devices, e.g. A_{Mobile} and A_{IoT} .

from different devices, e.g. IoT devices, and mobile phones, and it is larger than existing datasets. The main contributions of this work are summarized below.

- We propose a novel and simple loss term to narrow the cross-device gap at the pairwise level. We propose to use a ‘progressive target’ to guide the estimated histogram.
- We established a new cross-device palmprint benchmark to improve the study of cross-device RGB palmprint recognition based on existing datasets.
- Extensive experiments on the newly collected dataset and several existing palmprint recognition datasets verified the effectiveness of the proposed method.

We also tested the proposed method on cross-device person re-identification and the results are also in favor of our method.

The remaining of this paper is organized as follows. In Section 2, related studies are reviewed. Section 3 states the details of the proposed PTD loss. Experimental results and dataset details are presented in Section 4. Finally, Section 5 concludes the paper.

2. Related work

2.1. Traditional palmprint recognition methods

Traditional palmprint recognition methods can be roughly divided into two categories: (1) holistic-based and (2) local descriptor based. In holistic-based methods, features are extracted from the whole image and then projected to a latent space of lower-dimensional to make it more compact and discriminative. Supervised and unsupervised projection methods such as Principle Component Analysis (PCA) [5], Independent Component Analysis (ICA)

[6], Mix Factor Analysis (MFA) [7], and Linear Discriminant Analysis (LDA) [8] are used for dimension reduction. Gui et al. [9] use Locality Preserving Projection (LPP) to preserve local structures of palmprints. Hu et al. [10] extend LPP to 2D-LPP. Holistic-based methods often suffer from degradation caused by distortion, illumination, and noise. To overcome these issues, some studies try to transform the data from image domain to another domain. Frequency [11] and Cosine [12] transforms are commonly used to overcome these degradations.

Local descriptor based methods extract local features of the image and then construct a global description by feature fusion. The coding-based methods have the advantages of small storage space and fast processing speed, but the accuracy is slightly inferior. Earlier in [13], Zhang et al. designed the classic competitive code (CompCode) by using multiple 2-D Gabor filters to extract orientation information. FastCompCode [14] proposes a binary code for effective representation and matching. Li et al. [15] extract the local micro-structure tetra patterns. Jia et al. [16] propose the robust line orientation code (RLOC) [16]. Wu et al. [17] extract local SIFT features and match palm images with RANSAC. Qian et al. [18] extract histogram of orientations.

2.2. Deep learning for palmprint recognition.

Many recent studies use deep learning as feature extractor for palmprint recognition. In general, these deep learning based methods belong to holistic-based palmprint recognition. Dian et al. [19] first use the AlexNet as the feature extractor and match palm images with Hausdorff distance. Svoboda et al. [20] propose a new loss function related to the d-

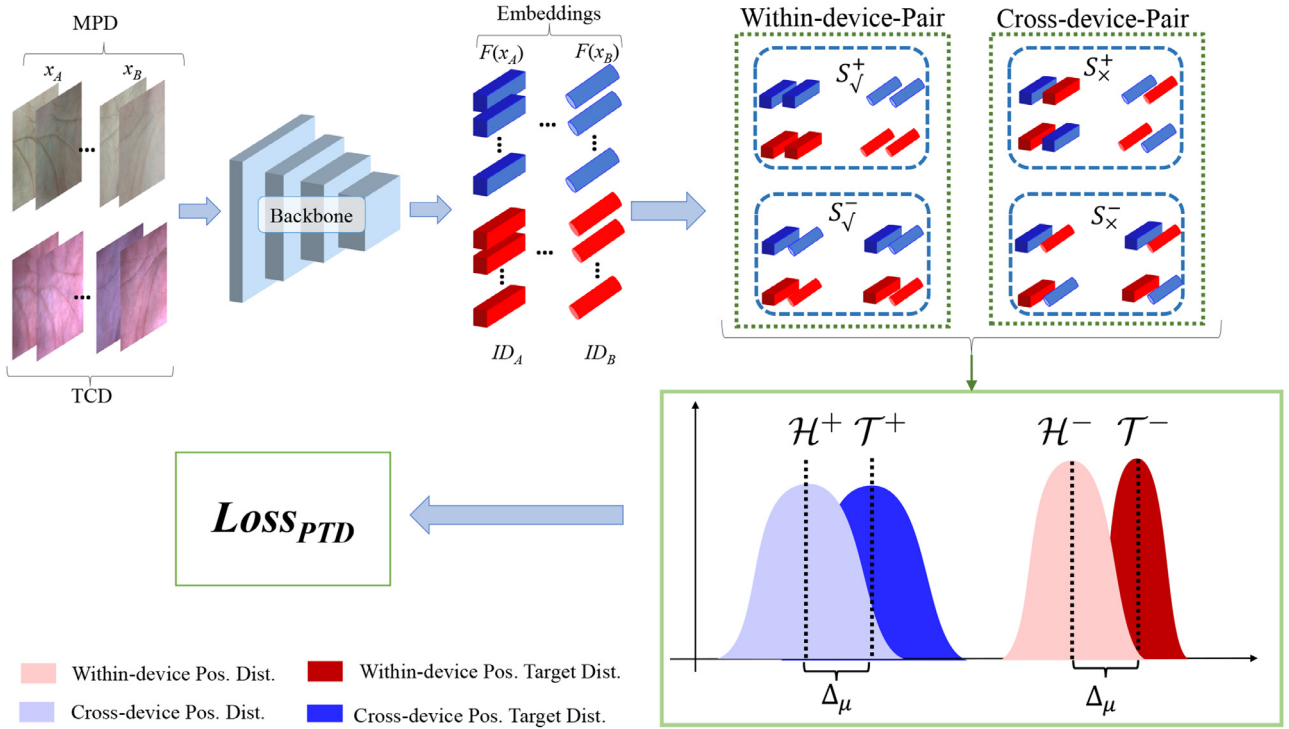


Fig. 2. Overall framework of the target distribution loss. During training, each mini-batch contains M IDs, and each ID contains N samples. Colors (red and blue) represent embeddings of different devices and shapes represent different identities.

prime index. Shao et al. [21] use deep metric learning to obtain discriminative features. Zhao et al. [22] design a novel CNN architecture for generic palmprint recognition in numerous scenarios. Recently, margin-based loss functions have been proven to be effective for face recognition. The large margin loss [23] and additive angular margin loss [3] are introduced to palmprint recognition. Fei et al. [24] propose a compact CNN-based surface representation for 3D palmprint recognition. Different from these studies that introduce new architectures or loss functions, our proposed method focuses on synthesizing training data for deep palmprint recognition.

3. Proposed method

As mentioned before, the heterogeneous visual characteristics existing between cross-device images pose a huge challenge. According to Fig. 1, the selected baseline ArcPalm [3] performs poorly in cross-device recognition scenarios. To solve the domain shift problem caused by heterogeneous image characteristics, we propose a PTD loss based on the baseline ArcPalm, which improves the cross-device recognition performance of the model by expanding the difference between the intra-class and inter-class similarity. The overall framework of the PTD loss is shown in Fig. 2. In this section, we will expand the principle and details of the PTD loss.

3.1. From pairwise similarity to histogram

Pairwise similarity. Let I be an arbitrary input image and F be the feature extractor, a convolutional neural network in our case. We denote the extracted features as $X = F(I)$, for simplicity we use X to represent a sample. The similarity between a pair of samples X_i, X_j is defined as their cosine distance in the embedding space:

$$s_{i,j} = \cos(X_i, X_j) = \frac{X_i \cdot X_j}{\|X_i\| \cdot \|X_j\|}.$$

Positive and negative pairs. Given an arbitrary pair of samples $\langle X_i, X_j \rangle$ and we denote their identity label as y_i, y_j . A pair is referred to as the *positive pair* if $y_i = y_j$ and otherwise the *negative pair*. Given a batch of samples $B = \{X_1, X_2, \dots, X_N\}$ where N is the batch size, we construct positive pairs and negative pairs according to their identity labels:

$$\begin{aligned} S^+ &= \{ \langle X_i, X_j \rangle \mid \forall X_i, X_{j,i \neq j} \in B, y_i = y_j \} \\ S^- &= \{ \langle X_i, X_j \rangle \mid \forall X_i, X_{j,i \neq j} \in B, y_i \neq y_j \}, \end{aligned} \quad (1)$$

where S^+ and S^- are the collections of positive/negative pairs. Note that the construction of positive pairs requires the sophisticated design of the batch sampler because if randomly sampled, there may be no positive pairs. More information about the batch sampler will be detailed in the experiments.

Cross-device and within-device pairs. Our proposed loss function can be used to improve cross-device palmprint recognition by pulling cross-device similarity of positive pairs. To this end, we have to build within-device and cross-device positive pairs. Given arbitrary sample X with identity label y , we denote its device as d . Then within-device and cross-device positive pairs are defined as:

$$\begin{aligned} S_V^+ &= \{ \forall \langle X_i, X_j \rangle \in S^+, d_i = d_j \} \\ S_X^+ &= \{ \forall \langle X_i, X_j \rangle \in S^+, d_i \neq d_j \} \\ S_V^- &= \{ \forall \langle X_i, X_j \rangle \in S^-, d_i = d_j \} \\ S_X^- &= \{ \forall \langle X_i, X_j \rangle \in S^-, d_i \neq d_j \}, \end{aligned} \quad (2)$$

where S_V represents the collection of within-device pairs and S_X is the collection of cross-device pairs.

Construct histograms. Next, we construct the histogram of positive and negative pairs according to their similarities. The ordinary discrete histogram is not decomposable and thus cannot be used in the CNN architecture for end-to-end optimization. Ustinova et al. [25] propose the histogram loss that builds decomposable histograms by interpolating between discrete values. Take positive pairs as an example, let $\mathcal{H}^+ \in \mathbb{R}^R$ be the histogram with

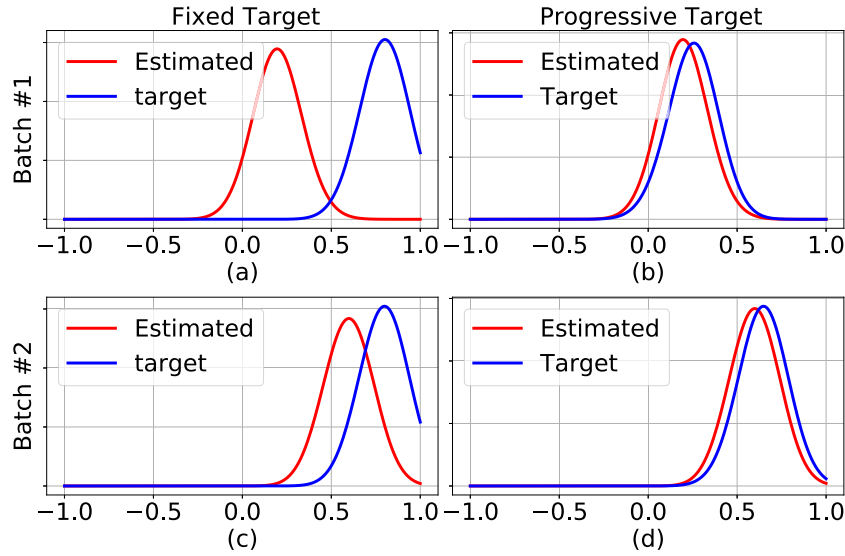


Fig. 3. Left: fixed distributional targets; Right: our proposed progressive targets. Top: Batch 1, Bottom: Batch 2.

nodes: $t_1 = -1, \dots, t_R = 1$. Where R is the dimension of the resulting histogram and the interval between two nodes is $\frac{2}{R-1}$. The r -th node of the histogram is:

$$h_r^+ = \frac{1}{|\mathcal{S}^+|} \sum_{(X_i, X_j) \in \mathcal{S}^+} \delta_{i,j,r}. \quad (3)$$

where

$$\delta_{i,j,r} = \begin{cases} (s_{ij} - t_{r-1})/\Delta; & \text{if } s_{ij} \in [t_{r-1}, t_r] \\ (t_{r+1} - s_{ij})/\Delta; & \text{if } s_{ij} \in [t_r, t_{r+1}] \\ 0; & \text{otherwise.} \end{cases} \quad (4)$$

Eq. 4 linearly interpolates between two nodes.

The histogram of negative similarities can be calculated analogously. We denote the positive/negative histogram as $\mathcal{H}^+, \mathcal{H}^- \in \mathbb{R}^R$.

Though the construction of histograms is inspired by [25], our proposed loss function is quite different from [25]: [25] tries to shrink the intersection between positive and negative histograms, our proposed method explicitly setup the target distribution for estimated histograms. Moreover, we propose *progressive targets* to smooth the ease the optimization.

3.2. Distributional loss with progressive targets

Distributional losses. After the positive/negative histograms are constructed, we set target distributions for them and then minimize the distance between histograms and their respective targets under specific metrics, e.g. KullbackLeibler divergence.

Let \mathcal{T} be the target distribution and \mathcal{H} be the estimated histogram. Our method minimizes the divergence between them:

$$\begin{aligned} \mathcal{L}_{hist}^+ &= D(\mathcal{H}^+, \mathcal{T}^+) \\ \mathcal{L}_{hist}^- &= D(\mathcal{H}^-, \mathcal{T}^-), \end{aligned} \quad (5)$$

where $D(\cdot, \cdot)$ is a distance metric on discrete distributions. In our experiments, we use KullbackLeibler divergence to measure the distributional distances for its simplicity.

Progressive Targets. Since the batch statistics vary very significantly during training, using a fixed target distribution may lead to difficulty in optimization and unstable results. As illustrated in Fig. 3 (a), when the estimated histogram is far away from the fixed target, the intersection of their support sets is nearly empty. Computing KL divergence under such conditions is an ill-posed problem. To avoid such a situation and make the training procedure

smooth, we propose the *progressive target* in the distribution-based loss.

Fig. 6 presents the similarity distributions of a single device dataset, PolyU, and the CrossDevice-A dataset. The similarities roughly follow a gaussian distribution. Therefore, we define the target histogram as a gaussian distribution with μ and σ differ a little bit from the estimated histograms. Specifically, let μ, σ be the mean and variance of the estimated histogram, the mean and the variance of its target distribution are given by:

$$\begin{aligned} \hat{\mu} &= \begin{cases} \mu + \Delta_\mu, & \text{if } \mathcal{H}^+ \\ \mu - \Delta_\mu, & \text{if } \mathcal{H}^- \end{cases} \\ \hat{\sigma} &= \mu - \Delta_\sigma, \end{aligned} \quad (6)$$

where $\Delta_\mu, \Delta_\sigma$ are small delta values.

Examples of the estimated histogram and target distribution can be found in Fig. 3 (b)&(d).

Total loss. In general, the final loss function consists of the *positive histogram loss* pull positive pairs, the *negative histogram loss* to push negative pairs, and the *ArcFace* for classification. In addition to the aforementioned terms, we add the *mean loss* to explicitly enlarge the average a similar gap between positive/negative pairs:

$$\mathcal{L}_{mean} = \text{mean}(\mathcal{H}^+) - \text{mean}(\mathcal{H}^-)$$

The total loss in our method can be formulated as:

$$\mathcal{L} = \alpha(\mathcal{L}_{hist}^+ + \mathcal{L}_{hist}^-) + \beta\mathcal{L}_{mean} + \mathcal{L}_{ArcFace}, \quad (7)$$

where α, β are balance factors.

The overall pipeline of the proposed method is summarized in line 1.

4. Cross device palm datasets

To the best of our knowledge, no palm dataset is dedicated to cross-device RGB palmprint recognition. Here ‘cross-device’ refers to RGB images that are taken by sensors, e.g. digital cameras, mobile phone, IoT devices et al. To fulfill the blank, we collect two cross-device palmprint recognition datasets, namely CrossDevice-A and CrossDevice-B, for improving the research of cross-device palm recognition. Example images of the newly collected dataset and their respective original datasets are shown in Fig. 4.



Fig. 4. Example images of the four source datasets. Each column represents images of the same identity taken by diverse devices.

Algorithm 1: Algorithmic outline of the proposed method.

Input: Model F , initial parameters Θ , learning rate α .

while not converged do

Random select a mini-batch B ;
 Collect sample pairs according to ~Eq. (1) or ~Eq. (2);
 Forward pass $F(B)$ to get features;
 Construct histogram \mathcal{H} according to ~Eq. (3);
 Get target distribution according to ~Eq. (6).
 Construct target distribution \mathcal{T} using $\hat{\mu}, \hat{\sigma}$;
 Compute loss according to ~Eq. (7)
 Backward to get gradient $\Delta\Theta$;
 Update Θ by: $\Theta := \Theta - \alpha \cdot \Delta\Theta$

end

Output: Θ

4.1. Data collection and annotation

CrossDevice-A. Images of CrossDevice-A are from MPD [3] and TCD [26] datasets where the images are taken by mobile and IoT devices, respectively. MPD and TCD datasets contain 400/600 identities and 16,000/12,000 images, respectively. As part of the identities present in both TCD and MPD, we construct CrossDevice-A by selecting intersect identities from TCD and MPD.

For each identity in MPD, we select top-5 candidate identities from TCD by computing the cosine similarity between identities. Formally, we define identity-level similarity as the average of instance-level similarities:

$$\mathcal{S}(\text{ID}^m, \text{ID}^n) = \frac{1}{\|\text{ID}^m\| \cdot \|\text{ID}^n\|} \sum_i \sum_j \cos(I_i^m, I_j^n),$$

where ID^m and ID^n are two identities and I_i^m (I_j^n) is the i -th (j -th) image in identity ID^m (ID^n). The instance-level similarity is computed based on features that are extracted using a pretrained palmprint recognition model.

After selecting top-5 most-similar identities, we manually verify and select the matched identity. The verification and selection is performed by two distinct human annotators for the sake of accuracy.

CrossDevice-B. Images of CrossDevice-B are from MOHI [27] and WEHI [27] datasets. Since the original MOHI and WEHI datasets are designated for hand shape recognition, therefore, the palmprint is not very clear. Consequently, the CrossDevice-B is more challenging than CrossDevice-A. The construction of CrossDevice-B is simpler than that of CrossDevice-

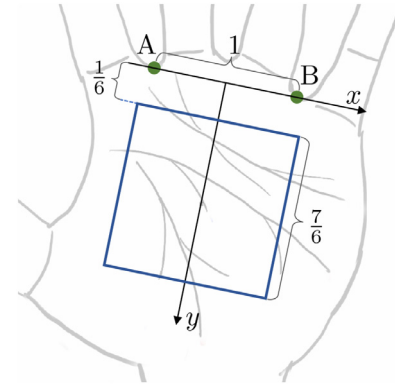


Fig. 5. ROI extraction of a left hand. We first detect two key points (green dots) A and B and then set up the coordinates where the x -axis is the line across A and B, and the y -axis is perpendicular. The ROI is a square on the upper half of y -axis.

B since the identities are strictly matched in the two source datasets.

The statistics of the two new datasets and their respective source datasets are summarized in Table 1.

5. Experiments

5.1. Implementation details

Training settings. Our method is implemented using the PyTorch framework. We first train a base model using the ArcFace loss and then finetune with ArcFace + PTD loss. The loss weights in PTD loss are set to: $\alpha = 2.0$, $\beta = 0.05$. The deltas in Eq. 6 are set to $\Delta\mu = 0.07$ and $\Delta\sigma = 0.05$. We train the model for 26 epochs in both first-round training and finetune. The initial learning rate is set to $5e^{-3}$ and the learning rate decays with a factor of 0.1 at 14, 18, and 24 epochs. We use the stochastic gradient descent algorithm to optimize the model, the movement is set to 0.9 and weight-decay is set to $5e^{-4}$. For more implementation details, please visit <https://kaizhao.net/palmprint>.

Datasets. We test our proposed method as well as competitors on CASIA [28], IITD [29], PolyU [30], TCD [26], MPD [3] and our newly collected datasets. Unless otherwise stated, we use the 5-fold cross-validation where 4/5 of images are used for training and others for testing. The statistics of these datasets are summarized in Tables 1 and 2.

ROI Extraction. Given a palm image, we first detect two landmarks and then crop the center area of the palm according to the landmarks. Fig. 5 illustrates the landmarks (A and B) and ROI of the left hand. As shown in Fig. 5, we use the intersection of the in-

Table 1
Statistics of two newly collected datasets and their respective source datasets.

New Dataset	#IDs	#samples	Source Dataset	#IDs	#samples	Device
CrossDevice-A	310	18,600	MPD	400	16,000	Mobile
			TCD	600	12,000	IoT
CrossDevice-B	200	6,000	MOHI	200	3000	Mobile
			WEHI	200	3000	WebCam

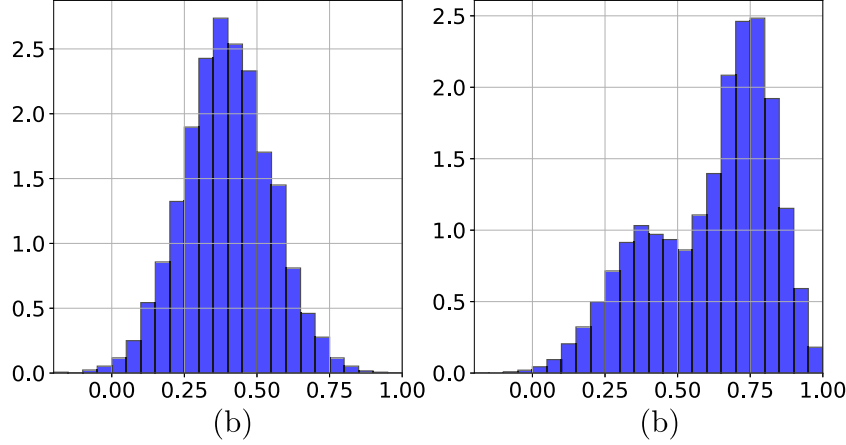


Fig. 6. (a) Histogram of positive similarities on single device dataset PolyU (b) Histogram of positive similarities on dual device dataset CrossDevice-A.

Table 2
Datasets used in our experiments for general palmprint recognition.

Datasets	Capture type	#images	#IDs
CASIA [28]	Contactless	5502	624
IITD [29]	Contactless	2601	460
PolyU [30]	Contactless	1140	114
TCD [26]	Contactless	12,000	600
MPD [3]	Smartphones	16,000	400

dex finger and little finger as the first landmark (A), and the intersection of the ring finger and middle finger as the second landmark (B). The landmarks are detected with a YOLOv3-based detector.

Network Architecture. Following the common practice of many previous studies [31], we use the Inception-ResNet (also known as Inception-v3) network as our backbone. Specifically, we use its 50 layer variant for the compromise between efficiency and performance, we will refer to the backbone network as ‘IR50’ for short.

Besides IR50, we took into account the limitations of computing power and speed requirements in some scenarios and selected MobileFaceNet [32] as Backbone to complete a series of experiments. In our experiments, MobileFaceNet was abbreviated as ‘MobileNet’.

We use the state-of-the-art loss function for face recognition, ArcFace [33], as the classification loss.

Evaluation protocol. We evaluate palmprint recognition results in terms of EER, TPR@FAR, and top-1 accuracy. When evaluating the cross-device setting, we use images of a device as a query and images of other devices as a gallery.

5.2. Results on general palmprint recognition.

In this section, we evaluated the performance of the baseline models on five public within-device palmprint datasets, and report it in Table 3 in detail. For all methods, we conduct 5-fold validation and record the average performance. Since the evaluation protocol of original papers vary significantly and almost each paper has its evaluation protocol, we put the results which strictly follow the original protocols in the supplementary material.

According to Table 3, the Top-1 Accuracy and EER of the baseline on each within-device dataset outperform the state-of-the-art methods. It can also be seen that based on the baseline ArcPalm, PTD can significantly improve performance. In particular, the Top-1 accuracy of the ArcPalm-IR+PTD achieved 100% on IITD, PolyU, and TCD, and close to 100% on CASIA and MPD.

5.3. Results on cross-device palmprint recognition.

Here we test our proposed method on the newly collected cross-device datasets: CrossDevice-A and CrossDevice-B.

Experimental settings. In the cross-device setting, we collect both cross-device positive pairs S_{χ}^{+} and within-device positive pairs S_{ψ}^{+} , as depicted in Eq. (2). As illustrated in Fig. 6 (b), the similarity histogram of positive similarities on cross-device dataset present dual-peak distribution, this reveals that we can model it with a mixture of Gaussians.

Based on the above intuition, we set up a target for cross-device and within-device pairs individually. Let S_{χ}^{+} and S_{ψ}^{+} be collection of cross-device positive similarities and within-device positive similarities. We setup two target distributions $\mathcal{T}_{\chi}^{+}, \mathcal{T}_{\psi}^{+}$ for them. The negative similarities $S_{\chi}^{-}, S_{\psi}^{-}$ and their targets $\mathcal{T}_{\chi}^{-}, \mathcal{T}_{\psi}^{-}$ are defined accordingly. Finally, the \mathcal{L}_{hist}^{+} and \mathcal{L}_{hist}^{-} in Eq. 5 are broken into two parts:

$$\begin{aligned}\mathcal{L}_{hist}^{+} &= D(\mathcal{H}_{\chi}^{+}, \mathcal{T}_{\chi}^{+}) + D(\mathcal{H}_{\psi}^{+}, \mathcal{T}_{\psi}^{+}) \\ \mathcal{L}_{hist}^{-} &= D(\mathcal{H}_{\chi}^{-}, \mathcal{T}_{\chi}^{-}) + D(\mathcal{H}_{\psi}^{-}, \mathcal{T}_{\psi}^{-}).\end{aligned}\quad (8)$$

During testing, we use images of one device as the gallery and images of the other device as registry to evaluate the cross-device recognition performance.

Quantitative evaluations The quantitative evaluation results are reported in Table 4. We compare the proposed method with several recent palmprint recognition methods such as PalmNet [34] and ArcPalm [3] using MobileNet [40] and Inception network [31] as backbone.

For CrossDevice-A, the Top-1 Accuracy of ArcPalm-IR50+PTD and ArcPalm-MobileNet+PTD are 0.4% and 2.15% higher than ArcPalm-IR50 and ArcPalm-MobileNet, respectively. While IR50+PTD’s EER and MobileNet’s EER are 0.22 and 0.92% lower.

Table 3

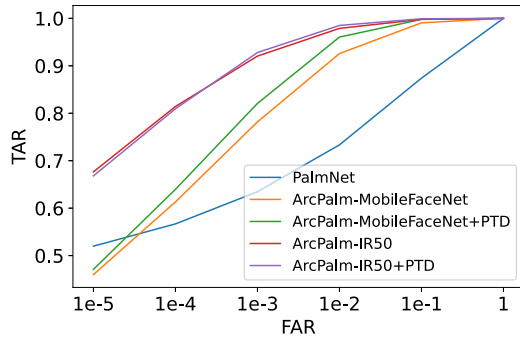
Top-1 Accuracy/EER (%) of the proposed method compared to other methods on several general palmprint recognition datasets.

Methods	CASIA	IITD	PolyU	TCD	MPD
PalmNet [34]	97.17 / 3.21	97.31 / 3.83	99.95 / 0.39	99.89 / 0.40	91.88 / 6.22
FERNet [35]	97.65 / 0.73	99.61 / 0.76	99.77 / 0.15	98.63 / -	- / -
DDBC [36]	96.41 / -	96.44 / -	-	98.73 / -	- / -
CompCode [13]	79.27 / 1.08	77.79 / 1.39	99.21 / 0.68	- / -	- / -
OLOF [37]	73.32 / 1.75	73.26 / 2.09	99.55 / 0.23	- / -	- / -
DoN [38]	99.30 / 0.53	99.15 / 0.68	100.00 / 0.22	- / -	- / -
C-LMCL [23]	- / -	- / -	100.00 / 0.13	99.93 / 0.26	- / -
JCLSR [39]	98.94 / -	98.17 / -	- / -	- / -	- / -
ArcPalm-IR50 [3]	98.91 / 0.59	99.85 / 0.47	100.00 / 0.08	99.90 / 0.21	99.18 / 0.81
ArcPalm-IR50 + PTD	99.85 / 0.37	100.00 / 0.20	100.00 / 0.05	100.00 / 0.04	99.78 / 0.43

Table 4

Top-1 accuracy and EER (%) of the ArcPalm-based methods under the cross-device evaluation protocol on CrossDevice-A and CrossDevice-B datasets. IR50 and MB indicate the IR50 and MobileFaceNet backbones, respectively.

Methods	CrossDevice-A		CrossDevice-B	
	Top-1	EER	Top-1	EER
PalmNet [34]	84.51	11.60	55.45	34.25
ArcPalm-MB	96.31	2.17	67.96	14.88
ArcPalm-MB+PTD	98.46	1.25	69.72	13.39
ArcPalm-IR50	98.79	1.17	67.63	14.62
ArcPalm-IR50+PTD	99.19	0.95	71.20	13.50

**Fig. 7.** ROC curve on crossPalm-A.

As for CrossDevice-B, it can be seen that IR50+PTD's Top-1 Accuracy is increased by 3.57%, and its EER is decreased by 1.12%. For MobileNet+PTD, its Top-1 Accuracy is increased by 1.76%, and its EER is decreased by 1.49%.

We drew the ROC curve of the SOTA method PalmNet [34], ArcPalm [3]-MobileNet, ArcPalm-MobileNet+PTD, ArcPalm-IR50, and ArcPalm-IR50+PTD on the CrossDevice-A dataset. According to Fig. 7, we can see that ArcPalm-X+PTD outperforms SOTA and its corresponding baseline model, which proves the effectiveness of our method.

5.4. Results on cross-dataset palmprint recognition

In this experiment, we test the cross-dataset generalization of our method. The model is trained on one dataset and evaluated on another dataset.

Results in Table 5 imply that our method show substantial advantages against the ArcPalm baseline under the challenging cross-dataset setting.

Table 5

Top-1 Accuracy (%) and EER (%) of the proposed method on cross-dataset recognition.

Method	Training	Test	Top-1	EER
C-LMCL [23]	TCD	PolyU	99.93	0.58
ArcPalm-IR50	TCD	PolyU	98.63	0.83
ArcPalm-IR50+PTD	TCD	PolyU	99.93	0.56
C-LMCL [23]	PolyU	TCD	98.72	1.46
ArcPalm-IR50	PolyU	TCD	97.09	1.74
ArcPalm-IR50+PTD	PolyU	TCD	98.74	1.43

Table 6

Ablation study of each components in Eq. 7 on the CrossDevice-A dataset.

\mathcal{L}_{hist}^+	\mathcal{L}_{hist}^-	\mathcal{L}_{mean}	EER	Top-1
×	×	×	96.31	2.17
×	×	✓	96.42	1.99
✓	✓	×	97.79	1.30
✓	✓	✓	98.46	1.25

Table 7

Ablation study of different target settings on CrossDevice-A (%). MB means using the MobileFaceNet as backbone.

Methods	Top-1	EER
ArcPalm-MB	96.31	2.17
ArcPalm-MB+Within-device Target *	96.75	1.94
ArcPalm-MB+Fixed Target	97.61	1.79
ArcPalm-MB+PTD	98.46	1.25

5.5. Ablation study

We conduct several ablation experiments to verify the effectiveness of the proposed method and test the robustness of our method against hyper-parameters. All experiments in this section are conducted on the CrossDevice-A dataset.

Effectiveness of each component. We first ablate the effectiveness of each component in Eq. 7. According to Table 6, each of our modules can improve the performance of the baseline model. Not only that, the Top-1 accuracy and EER including the PTD loss of all modules are the best, indicating that each module is an indispensable part of the PTD loss.

PTD v.s. fixed targets. In the first experiments, we verify the effectiveness of the proposed method by comparing the performance of PTD and a counterpart with a fixed target. According to Table 7, PTD outperforms fixed target in terms of both Top-1 accuracy and EER. When using within-device distribution as the target, its performance is not as good as the proposed PTD loss. Therefore, we believe that the PTD loss target setting is more reasonable and effective. For the fixed target counterpart, we set up a fixed target for positive/negative pairs, respectively. We set $\mu = 0.7, \sigma = 0.01$ for

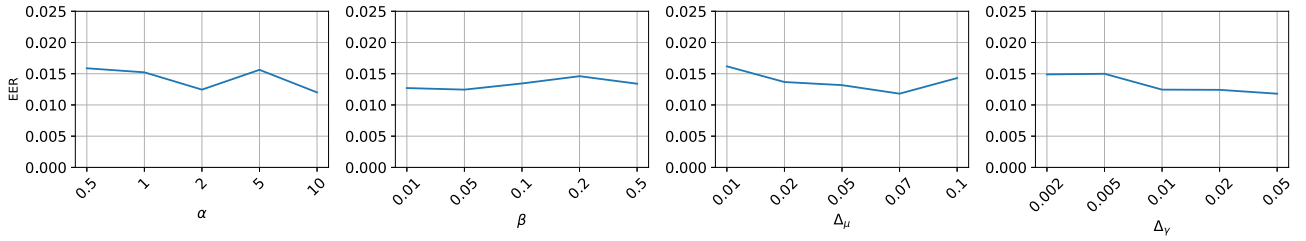


Fig. 8. Performance (EER) of our method with different hyper-parameters. When tuning one hyper-parameter, we fix others to the default value.

Table 8
Evaluations (%) of PTD loss on SYSU-MM01 [44] dataset.

Method	All Search		Indoor Search	
	Rank-1	mAP	Rank-1	mAP
PIG [41]	45.10	25.50	52.70	42.70
SIM [42]	57.47	53.75	-	-
DDAG [42]	54.75	53.02	61.02	67.98
AGW [43]	47.50	47.65	54.17	59.81
AGW+PTD	60.13	57.42	62.51	70.64

Table 9
Evaluations (%) of PTD loss on RegDB [46] dataset.

Method	Visible to Infrared		Infrared to Visible	
	Rank-1	mAP	Rank-1	mAP
PIG [41]	48.50	49.30	48.10	48.90
SIM [42]	75.29	74.47	78.30	75.24
DDAG [45]	68.06	61.80	69.34	63.46
AGW [43]	70.05	66.37	-	-
AGW+PTD	78.73	78.12	79.63	77.84

positive pairs and $\mu = 0, \sigma = 0.01$ for negative pairs. Results are in Table 7.

PTD under different hyper-parameters. Here we report the performance of PTD under different hyper-parameters, these hyper-parameters are: loss weights α, β in Eq. 7 and deltas $\Delta\mu, \Delta\sigma$ in Eq. 6. When tuning one hyper-parameter, we fix others as the default values. The results in Fig. 8 reveal that our method is robust against the choice of loss weights α, β and deltas $\Delta\mu, \Delta\sigma$.

5.6. Experiments on person re-identification

Person re-identification (ReID) is a similar task which aims to learning discriminative features to identity pedestrians. Recently, many deep learning based ReID methods have been proposed [43,47,48]. To further verify the generalization of our proposed method, we also test our method on cross-device person re-identification. task. We use the AGW [43] as the baseline to verify the effectiveness of our method. The experiments on ReID are conducted on SYSU-MM01 [44] and RegDB [46] datasets. The images of SYSU-MM01 dataset are captured by RGB cameras under two scenes: indoor and outdoor. We evaluate both the all-to-all and the indoor-to-outdoor performance. The RegDB is a cross-device and cross-modal dataset that the images are captured by RGB (visible) and infrared cameras. We evaluate all-to-all and the infrared-to-visible performance on RegDB dataset. The results in Tables 8 and 9 clearly demonstrate that our method consistently improves the performance of a strong baseline with considerable margins.

6. Conclusion and future work

In this paper, we propose a new loss function for cross-device palmprint recognition. Our contributions are summarized as fol-

lows. We first reorganized a large-scale palm benchmark dataset consists of two subsets. Second, we propose the progressive target loss (PTD loss) which progressively narrows the gap between representations of cross-device samples. Extensive experiments have demonstrated the superior of our method. The proposed dataset will benefit the research of cross-device palmprint recognition, and the proposed method may be also helpful to other biometric recognition tasks, e.g. face recognition. Though it is effective, our method works in a supervised manner which means the device labels are required during training, which limits its application to unsupervised conditions where device labels are unavailable. Besides, our method brings extra computation to estimate the distribution of sample similarities.

Declaration of Competing Interest

The authors declare that they have no known competing financial interests or personal relationships that could have appeared to influence the work reported in this paper.

References

- [1] Amazon ONE, (<https://one.amazon.com/>).
- [2] L. Fei, G. Lu, W. Jia, S. Teng, D. Zhang, Feature extraction methods for palmprint recognition: a survey and evaluation, IEEE Trans. Syst. Man Cybern. Syst. 49 (2) (2018) 346–363, doi:10.1109/TSMC.2018.2795609.
- [3] Y. Zhang, L. Zhang, R. Zhang, S. Li, J. Li, F. Huang, Towards palmprint verification on smartphones, arXiv preprint arXiv:2003.13266(2020).
- [4] H. Shao, D. Zhong, X. Du, Efficient deep palmprint recognition via distilled hashing coding, in: Proceedings of the IEEE Conference on Computer Vision and Pattern Recognition Workshops, IEEE, Long Beach, CA, USA, 2019, pp. 0–0. 10.1109/CVPRW.2019.00098.
- [5] G. Lu, D. Zhang, K. Wang, Palmprint recognition using eigenpalms features 24(9–10) (2003) 1463–1467.
- [6] T. Connie, A.T.B. Jin, M.G.K. Ong, D.N.C. Ling, An automated palmprint recognition system, Image Vis Comput 23 (5) (2005) 501–515.
- [7] J. Chen, L. Liao, W. Zhang, L. Du, Mixture factor analysis with distance metric constraint for dimensionality reduction, Pattern Recognit 121 (2022) 108156.
- [8] M. Wang, Q. Ruan, Palmprint recognition based on two-dimensional methods, in: Proceedings of the ICSP, volume 4, IEEE, 2006.
- [9] J. Gui, W. Jia, L. Zhu, S.-L. Wang, D.-S. Huang, Locality preserving discriminant projections for face and palmprint recognition, Neurocomputing 73 (13–15) (2010) 2696–2707.
- [10] D. Hu, G. Feng, Z. Zhou, Two-dimensional locality preserving projections (2DLPP) with its application to palmprint recognition, Pattern Recognit 40 (1) (2007) 339–342.
- [11] H. Li, L. Wang, Palmprint recognition using dual-tree complex wavelet transform and compressed sensing, in: Proceedings of the 2012 International Conference on Measurement, Information and Control, volume 2, IEEE, 2012, pp. 563–567.
- [12] L. Leng, M. Li, C. Kim, X. Bi, Dual-source discrimination power analysis for multi-instance contactless palmprint recognition, Multimed. Tools Appl. 76 (1) (2017) 333–354.
- [13] A.-K. Kong, D. Zhang, Competitive coding scheme for palmprint verification, in: Proceedings of the 17th International Conference on Pattern Recognition, in: ICPR '17, volume 1, IEEE, Cambridge, UK, 2004, pp. 520–523, doi:10.1109/ICPR.2004.1334184.
- [14] Q. Zheng, A. Kumar, G. Pan, Suspecting less and doing better: new insights on palmprint identification for faster and more accurate matching, IEEE TIFS 11 (3) (2015) 633–641.
- [15] G. Li, J. Kim, Palmprint recognition with local micro-structure tetra pattern, Pattern Recognit 61 (2017) 29–46.
- [16] W. Jia, D.-S. Huang, D. Zhang, Palmprint verification based on robust line orientation code, Pattern Recognit 41 (5) (2008) 1504–1513.

- [17] X. Wu, Q. Zhao, W. Bu, A SIFT-based contactless palmprint verification approach using iterative RANSAC and local palmprint descriptors, *Pattern Recognit* 47 (10) (2014) 3314–3326.
- [18] J. Qian, J. Yang, G. Gao, Discriminative histograms of local dominant orientation (d-HLDO) for biometric image feature extraction, *Pattern Recognit* 46 (10) (2013) 2724–2739.
- [19] L. Dian, S. Dongmei, Contactless palmprint recognition based on convolutional neural network, in: *Proceedings of the IEEE ICSP, IEEE*, 2016, pp. 1363–1367.
- [20] J. Svoboda, J. Masci, M.M. Bronstein, Palmprint recognition via discriminative index learning, in: *Proceedings of the 23rd International Conference on Pattern Recognition*, in: *ICPR '16, IEEE*, Cancun, Mexico, 2016, pp. 4232–4237, doi:10.1109/ICPR.2016.7900298.
- [21] H. Shao, D. Zhong, Towards open-set touchless palmprint recognition via weight-based meta metric learning, *Pattern Recognit* 121 (2022) 108247.
- [22] S. Zhao, B. Zhang, Deep discriminative representation for generic palmprint recognition, *Pattern Recognit* 98 (2020) 107071.
- [23] D. Zhong, J. Zhu, Centralized large margin cosine loss for open-set deep palmprint recognition, *IEEE Trans. Circuits Syst. Video Technol.* (2019), doi:10.1109/TCSVT.2019.2904283.
- [24] L. Fei, B. Zhang, Y. Xu, W. Jia, J. Wen, J. Wu, Precision direction and compact surface type representation for 3d palmprint identification, *Pattern Recognit* 87 (2019) 237–247.
- [25] E. Ustinova, V. Lempitsky, Learning deep embeddings with histogram loss, in: *Proceedings of the Advances in Neural Information Processing Systems*, in: *NIPS '16, Curran Associates, Inc., Barcelona, SPAIN*, 2016, pp. 4170–4178.
- [26] L. Zhang, L. Li, A. Yang, Y. Shen, M. Yang, Towards contactless palmprint recognition: a novel device, a new benchmark, and a collaborative representation based identification approach, *Pattern Recognit.* 69 (2017) 199–212, doi:10.1016/j.patcog.2017.04.016.
- [27] A. Hassanat, M. Al-Awadi, E. Btoush, A. Al-Btoush, E. Alhasanat, G. Altarawneh, New mobile phone and webcam hand images databases for personal authentication and identification, *Procedia Manuf.* 3 (2015) 4060–4067, doi:10.1016/j.promfg.2015.07.977.
- [28] Y. Hao, Z. Sun, T. Tan, C. Ren, Multispectral palm image fusion for accurate contact-free palmprint recognition, in: *Proceedings of the 15th IEEE International Conference on Image Processing*, in: *ICIP '08, IEEE*, San Diego, CA, USA, 2008, pp. 281–284, doi:10.1109/ICIP.2008.4711746.
- [29] A. Kumar, Incorporating cohort information for reliable palmprint authentication, in: *Proceedings of the 6th Indian Conference on Computer Vision, Graphics and Image Processing*, in: *ICVGIP '08, IEEE*, Bhubaneswar, India, 2008, pp. 583–590, doi:10.1109/ICVGIP.2008.73.
- [30] V. Kanhangad, A. Kumar, D. Zhang, Contactless and pose invariant biometric identification using hand surface, *IEEE Trans. Image Process.* 20 (5) (2010) 1415–1424, doi:10.1109/TIP.2010.2090888.
- [31] C. Szegedy, S. Ioffe, V. Vanhoucke, A.A. Alemi, Inception-v4, inception-resnet and the impact of residual connections on learning, in: *Proceedings of the 31st AAAI conference on artificial intelligence*, in: *AAAI '17, 2017*, pp. 4278–4284. San Francisco, CA, USA
- [32] S. Chen, Y. Liu, X. Gao, Z. Han, MobileFaceNets: efficient CNNs for accurate real-time face verification on mobile devices, in: *Proceedings of the Chinese Conference on Biometric Recognition*, in: *CVBR '18, Springer*, Xinjiang, China, 2018, pp. 428–438, doi:10.1007/978-3-319-97909-0_46.
- [33] J. Deng, J. Guo, N. Xue, S. Zafeiriou, Arcface: Additive angular margin loss for deep face recognition, in: *Proceedings of the IEEE*, in: *CVPR '19, 2019*, pp. 4690–4699, doi:10.1109/CVPR.2019.00482.
- [34] A. Genovese, V. Piuri, K.N. Plataniotis, F. Scotti, Palmnet: gabor-PCA convolutional networks for touchless palmprint recognition, *IEEE Trans. Inform. Forensics Secur.* 14 (12) (2019) 3160–3174, doi:10.1109/TIFS.2019.2911165.
- [35] W.M. Matkowski, T. Chai, A.W.K. Kong, Palmprint recognition in uncontrolled and uncooperative environment, *IEEE Trans. Inform. Forensics Secur.* (2019), doi:10.1109/TIFS.2019.2945183.
- [36] L. Fei, B. Zhang, Y. Xu, Z. Guo, J. Wen, W. Jia, Learning discriminant direction binary palmprint descriptor, *IEEE Trans. Image Process.* 28 (8) (2019) 3808–3820, doi:10.1109/TIP.2019.2903307.
- [37] Z. Sun, T. Tan, Y. Wang, S.Z. Li, Ordinal palmprint representation for personal identification [representation read representation], in: *Proceedings of the IEEE Computer society Conference on Computer Vision and Pattern Recognition*, in: *CVPR '05, volume 1, IEEE*, San Diego, CA, USA, 2005, pp. 279–284, doi:10.1109/CVPR.2005.267.
- [38] Q. Zheng, A. Kumar, G. Pan, A 3d feature descriptor recovered from a single 2d palmprint image, *IEEE Trans. Pattern Anal. Mach. Intell.* 38 (6) (2016) 1272–1279.
- [39] S. Zhao, B. Zhang, Joint constrained least-square regression with deep convolutional feature for palmprint recognition, *IEEE Trans. Syst. Man Cybernet. Syst.* (2020).
- [40] M. Sandler, A. Howard, M. Zhu, A. Zhmoginov, L.-C. Chen, Mobilenetv2: Inverted residuals and linear bottlenecks, 2018, pp. 4510–4520.
- [41] M. Jia, Y. Zhai, S. Lu, S. Ma, J. Zhang, A similarity inference metric for RGB-infrared cross-modality person re-identification, in: *Proceedings of the 29th International Joint Conference on Artificial Intelligence*, in: *IJCAI '20, AAAI Press*, 2020, pp. 1026–1032, doi:10.24963/ijcai.2020/143.
- [42] G.-A. Wang, T. Zhang, Y. Yang, J. Cheng, J. Chang, X. Liang, Z.-G. Hou, Cross-modality paired-images generation for RGB-infrared person re-identification, in: *Proceedings of the AAAI Conference on Artificial Intelligence*, volume 34, AAAI Press, 2020, pp. 12144–12151, doi:10.1609/aaai.v34i07.6894.
- [43] M. Ye, J. Shen, G. Lin, T. Xiang, L. Shao, S.C.H. Hoi, Deep learning for person re-identification: a survey and outlook, *IEEE Trans. Pattern Anal. Mach. Intell.* (2021).
- [44] A. Wu, W.-S. Zheng, H.-X. Yu, S. Gong, J. Lai, Rgb-infrared cross-modality person re-identification, in: *Proceedings of the IEEE international conference on computer vision*, 2017, pp. 5380–5389.
- [45] M. Ye, J. Shen, D.J. Crandall, L. Shao, J. Luo, Dynamic dual-attentive aggregation learning for visible-infrared person re-identification, in: *Proceedings of the European Conference on Computer Vision*, in: *ECCV '20, Springer*, 2020.
- [46] D.T. Nguyen, H.G. Hong, K.W. Kim, K.R. Park, Person recognition system based on a combination of body images from visible light and thermal cameras, *Sensors* 17 (3) (2017) 605.
- [47] Y. Chen, H. Wang, X. Sun, B. Fan, C. Tang, H. Zeng, Deep attention aware feature learning for person re-identification, *Pattern Recognit.* 126 (2022) 108567.
- [48] F. Yang, K. Yan, S. Lu, H. Jia, X. Xie, W. Gao, Attention driven person re-identification, *Pattern Recognit.* 86 (2019) 143–155.

Lei Shen is currently a researcher at Tencent Youtu Lab. He received his master degree in biomedical engineering from Fudan University, China. His research interests are artificial intelligence and computer vision, with a special focus on metric learning and recognition.

Yingyi Zhang is currently a researcher at Tencent Youtu Lab. She received her master degree in computer science from Fudan University, China. Her research interests lie in computer vision and image processing.

Kai Zhao is currently a postdoctoral researcher at University of California, Los Angeles. He received his PhD degree from the college of computer science, Nankai University in 2020. Before that, he received B.S. and M.S. from Shanghai University in 2014 and 2017, respectively. He has over 10 peer-reviewed publications in computer vision and machine learning related areas, including *IEEE Trans. PAMI*, *IEEE Trans. Image Processing*, *NeurIPS*, *ICCV*, *CVPR*, *ECCV* and *IJCAI*. More information can be found on his homepage <http://kaizhao.net>.

Ruixin Zhang is currently a senior researcher at Tencent Youtu Lab. He received his master degree in EE from Shanghai Jiaotong University, China. His research interests are computer vision and image processing.

Wei Shen Wei Shen is a tenure-track Associate Professor at the Artificial Intelligence Institute, Shanghai Jiao Tong University, since October 2020. Before that, he was an Assistant Research Professor at the Department of Computer Science, Johns Hopkins University, worked with Bloomberg Distinguished Professor Alan Yuille. He received his B.S. and Ph.D. degrees from Huazhong University of Science and Technology in 2007 and in 2012, respectively. In 2012, he joined Shanghai University, served as an Assistant Professor and then an Associate Professor until Oct 2018. He also worked as a research intern with Prof. Zhuowen Tu at Microsoft Research Asia. He has over 50 peer-reviewed publications in computer vision and machine learning related areas, including *IEEE Trans. PAMI*, *IEEE Trans. Image Processing*, *IEEE Trans. Medical Imaging*, *NIPS*, *ICML*, *ICCV*, *CVPR*, *ECCV* and *MICCAI*. He is an Area Chair for *CVPR* 2022 and a Senior Program Committee (SPC) Member for *AAAI* 2022.